Vapor–Solid Growth of One-Dimensional Layer-Structured Gallium Sulfide Nanostructures

Guozhen Shen,[†,‡,*] Di Chen,[†] Po-Chiang Chen,[‡] and Chongwu Zhou[‡]

[†]Wuhan National Laboratory for Optoelectronics and College of Optoelectronic Science and Engineering, Huazhong University of Science and Technology, Wuhan 430074, P. R. China, and [‡]Department of Electrical Engineering, University of Southern California, Los Angeles, California 90089

ABSTRACT Gallium sulfide (GaS) is a wide direct bandgap semiconductor with uniform layered structure used in photoelectric devices, electrical sensors, and nonlinear optical applications. We report here the controlled synthesis of various high-quality one-dimensional GaS nanostructures (thin nanowires, nanobelts, and zigzag nanobelts) as well as other kinds of GaS products (microbelts, hexagonal microplates, and GaS/Ga_2O_3 heterostructured nanobelts) *via* a simple vapor–solid method. The morphology and structures of the products can be easily controlled by substrate temperature and evaporation source. Optical properties of GaS thin nanowires and nanobelts were investigated and both show an emission band centered at 580 nm.

KEYWORDS: GaS · nanowires · semiconductor · nanobelts · photoluminescence

Gallium sulfide (GaS) is one of the most important wide bandgap III–VI semiconductors (E_g = 3.05 eV) with layered structures.[1] GaS usually crystallizes into double layers of nonmetal atoms, each consisting of [S–Ga–Ga–S] sheets and stacking together by the nonbonding interaction through the S atoms along the *c*-axis as shown in Figure 1 inset.[1] There are two layers in a single GaS unit cell, in which the bonding between two adjacent layers is the van der Waal interaction and the bonding within a layer is predominantly covalent. The strong intralayer bonding and the weak interlayer van der Waals interaction give rise to highly anisotropic structural, electrical, optical, and mechanical properties, which have made GaS attractive in photoelectric devices, electrical sensors, and nonlinear optical applications. For example, doped GaS is a promising material for the fabrication of near-blue-light emitting devices.[2] Thin films of GaS deposited on GaAs substrate can enhance photoluminescence yield of GaAs by 2 orders of magnitude.[3]

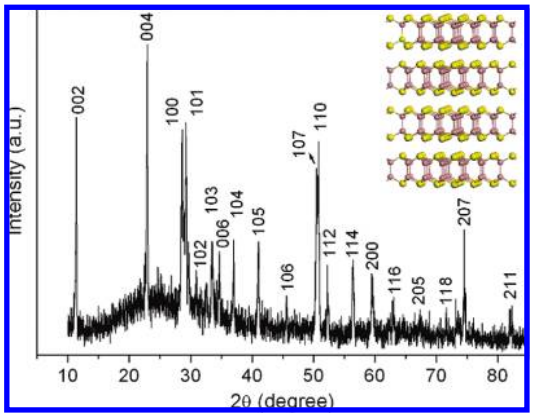

Figure 1. Typical XRD pattern of a GaS nanostructure. Inset: structural model of GaS with layered structure.

One-dimensional (1-D) nanowires, nanotubes and nanobelts recently became the focus of intensive research to be used as active materials for high-performance nanoscale devices due to their unique structures, such as large surface-to-volume ratios.[4–17] Both theoretical work and experimental work have been done on 1-D GaS nanostructures.[18–23] GaS nanotubes were theoretically predicted and they might find uses in nanoscale devices.[18] The mechanical properties of GaS nanotubes are believed to relate with the tube diameter and wall thickness.[18] Using a laser and thermally induced exfoliation method, Gautam et al. synthesized GaS nanotubes.[19] Hu et al. also synthesized GaS nanotubes using a thermal annealing method.[20] Both methods created nanotubes with bad crystallinity, which may greatly affect their semiconducting performance and future applications. Very recently, Hu *et al.* synthesized high-quality GaS submicrotubes using a high-temperature thermal reaction method at 1400–1500 °C[21,22] and Panda *et al.* synthesized short GaS nanobelts using catalyst-assisted thermal evaporation method.[23] Using these two methods, high-

*Address correspondence to gzshen@ustc.edu, gzshen@mail.hust.edu.cn.

Received for review February 10, 2009 and accepted April 01, 2009.

Published online April 8, 2009.
10.1021/nn900133f CCC: $40.75

© 2009 American Chemical Society

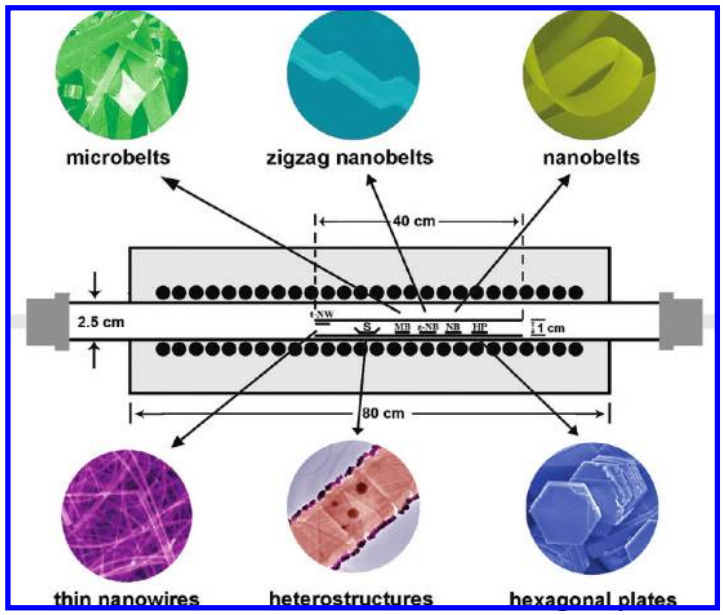

Scheme 1. Vapor−solid method used for the controlled growth of 1-D GaS nanostructures.

quality GaS nanostructures were produced. However, systematic studies on the controlled growth of 1-D GaS nanostructures with different morphologies are still not available until now.

Herein, using a simple catalyst-free vapor−solid method, we reported the controlled synthesis of high-quality GaS nanostructures on a large scale. We were able to control the morphologies (thin nanowires, nanobelts, zigzag nanobelts, microbelts, hexagonal microplates) and compositions of the GaS products (heterostructured nanobelts) by substrate temperature as well as evaporation source. The strategy utilized for controllable growth of GaS products is illustrated in Scheme 1.

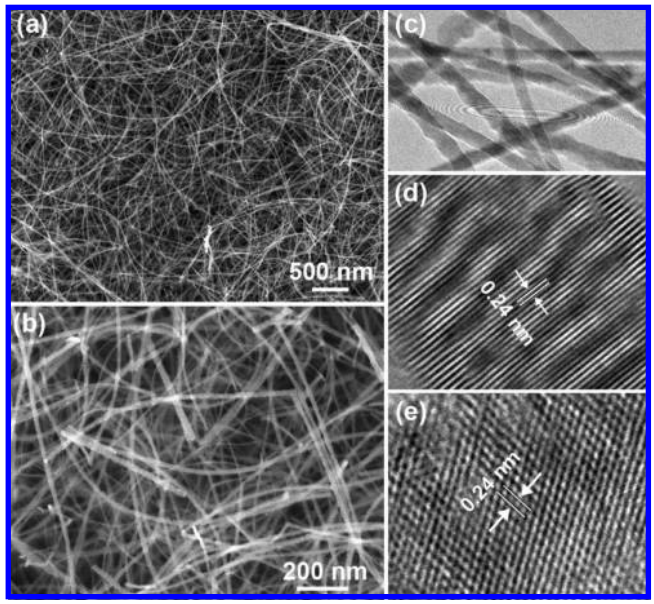

Figure 2. (a,b) SEM images, (c) TEM image, and (d,e) HRTEM images of the thin GaS nanowires.

RESULTS AND DISCUSSION

Figure 1 shows an XRD pattern of a typical product. All peaks in this pattern can be indexed to pure hexagonal GaS (JCPDS NO. 30-0576, space group: $P6_3/mmc$). During XRD analysis, no characteristic peaks from other crystalline impurities, such as GaN, Ga_2O_3, Bi_2S_3, were detected, indicating the formation of high purity GaS products.

Figures 2 panels a and b show the SEM images with different magnifications of the GaS product deposited on the upstream end of the inner wall of the small quartz tube as indicated in Scheme 1. It can be clearly seen that the product deposited here consists exclusively of thin nanowires with lengths of several micrometers on a large scale (Supporting Information, Figure S1). A typical TEM image of the thin GaS nanowires is shown in Figure 2c. It shows that the thin GaS nanowires have uniform diameters of ~20 nm. EDS attached to TEM was used to check the composition of nanowires and the spectrum shows the presence of Ga and S, indicating the formation of GaS (Supporting Information, Figure S2). High-resolution TEM (HRTEM) was used to study the microstructures of the thin GaS nanowires, and the lattice-resolved HRTEM images taken from two typical thin GaS nanowires are depicted in Figure 2d,e. These nanowires are of single crystal nature and the clearly marked interplanar *d* spacing is calculated to be 0.24 nm, which corresponds to that of the [104] lattice plane of hexagonal GaS. Defects were found to exist in the nanowires as revealed by the images.

The substrate temperature where the products deposited plays an important role in the formation of GaS nanostructures with different morphologies. Figure 3a shows a low-magnification SEM image of the GaS products deposited on the graphite substrate downstream where the temperature is around 800 °C. According to the high-resolution SEM images (Figure 3b−f), the products are composed of numerous nanobelts with typical lengths of several tens to hundred micrometers. Detailed analysis reveals that most of the GaS nanobelts are of branched comblike morphologies instead of forming individual nanobelts (Figure 3b and 3c). In other words, for the present GaS products, many GaS nanobelts grew on either one side (Figure 3b) or both sides (Figure 3c) of a stem GaS nanobelt. Figure 3d is a SEM image of several aligned GaS nanobelts grown on one side of a single GaS comb. According to these images, typical GaS nanobelts have rough surfaces and widths of 1−2 μm. The thickness of these GaS nanobelts can be calculated from the side-view SEM images shown in Figures 3e,f, where the beltlike morphology is well recognized. Typical GaS nanobelts have thicknesses of 70−80 nm. Besides GaS nanobelts with rough surfaces, some GaS nanobelts with smooth surfaces were also detected, which are usually highly curved as revealed in Figure 3g,h.

To study the microstructures of these GaS nanobelts, TEM, HRTEM, and selected-area electron diffraction (SAED) were performed. Figure 4a is a TEM image of two individual GaS nanobelts with widths of about 1 μm. Both nanobelts have rough surfaces similar to the SEM results in Figure 3d. The branched structure can be clearly seen in Figure 4b. The insets in this image are SAED patterns taken from different regions of the branched nanobelts, revealing the single crystal nature of both nanobelts. Both patterns can be indexed as the [001] zone axis of a hexagonal GaS crystal. Lattice-resolved HRTEM were taken on different regions marked in Figure 4b and the corresponding images are depicted in Figures 4c−e. The resolved lattice fringes in these images are about 0.31 nm, corresponding well to the (101) plane of hexagonal GaS crystal. On the basis of the SAED patterns and the HRTEM images, we can deduce that the preferred growth directions of the GaS nanobelts are perpendicular to the {100} planes. Figure 4f is a TEM image of a GaS nanobelt with smooth surface. The corresponding SAED pattern shown in the inset can also be indexed to the [001] zone axis of a hexagonal GaS crystal. The HRTEM image of the smooth GaS nanobelt is shown in Figure 4g, where the calculated lattice distance is 0.31 nm, also corresponding to the (101) plane of hexagonal GaS. The results indicate that the growth directions for these nanobelts are along the [100] orientations.

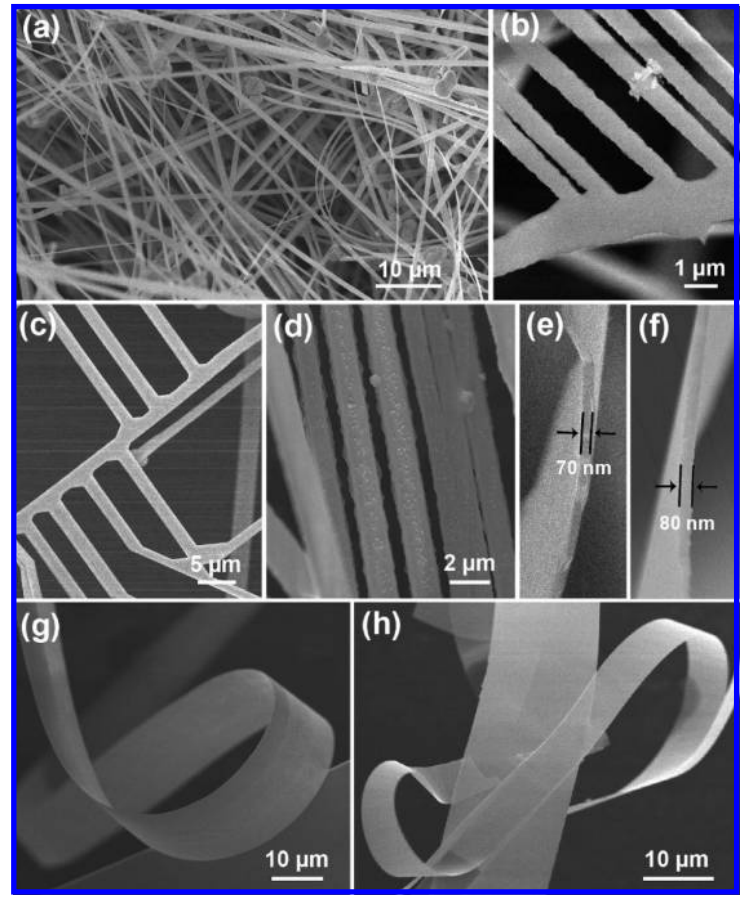

Figure 3. (a) Low-magnification SEM image of GaS nanobelts; (b−d) high-magnification SEM images of the GaS nanobelts, showing interesting branched structures composed of aligned nanobelts; (e,f) side-view SEM images of the GaS nanobelts, showing thin belt-thickness; (g,h) highly curved GaS nanobelts.

On the substrate where the temperature is around 800−850 °C, many zigzag GaS nanobelts were found deposited besides the straight nanobelts discussed above. Figure 5 panels a and b are SEM images of several zigzag GaS nanobelts with widths of 1−2 μm. The belt shape of the zigzag GaS nanobelt can be clearly seen in Figure 5c. We also studied the microstructures of the zigzag GaS nanobelts using TEM, HRTEM, and SAED, and the results are demonstrated in Figure 5d−f. Figure 5d is a TEM image showing four kinks of a zigzag GaS nanobelt. The angle between two neighboring kinks is calculated to be 120°, which is in consistent with that between two {101} planes of hexagonal GaS. A high-magnification TEM image taken on the edge of a single kink is depicted in Figure 5e. From this image, one can see that the GaS nanobelt is wrapped with a layer of amorphous material with thickness of several nanometers. The corresponding SAED pattern taken from the kink is shown in Figure 5e inset, which can also be indexed to the [001] zone axis of hexagonal GaS. Undoubtedly, the observed lattice fringes are separated by 0.31 nm, in according to the (101) plane of hexagonal GaS.

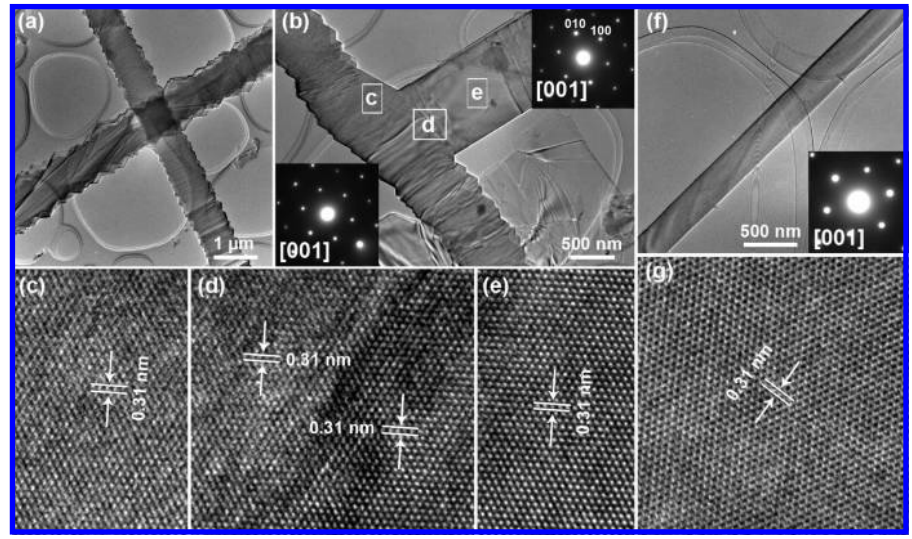

Figure 4. (a) TEM image of two GaS nanobelts; (b) TEM image of a branched GaS nanobelt; (c−e) HRTEM images taken from the parts framed in panel b; (f) TEM image and (g) HRTEM image of a straight GaS nanobelt.

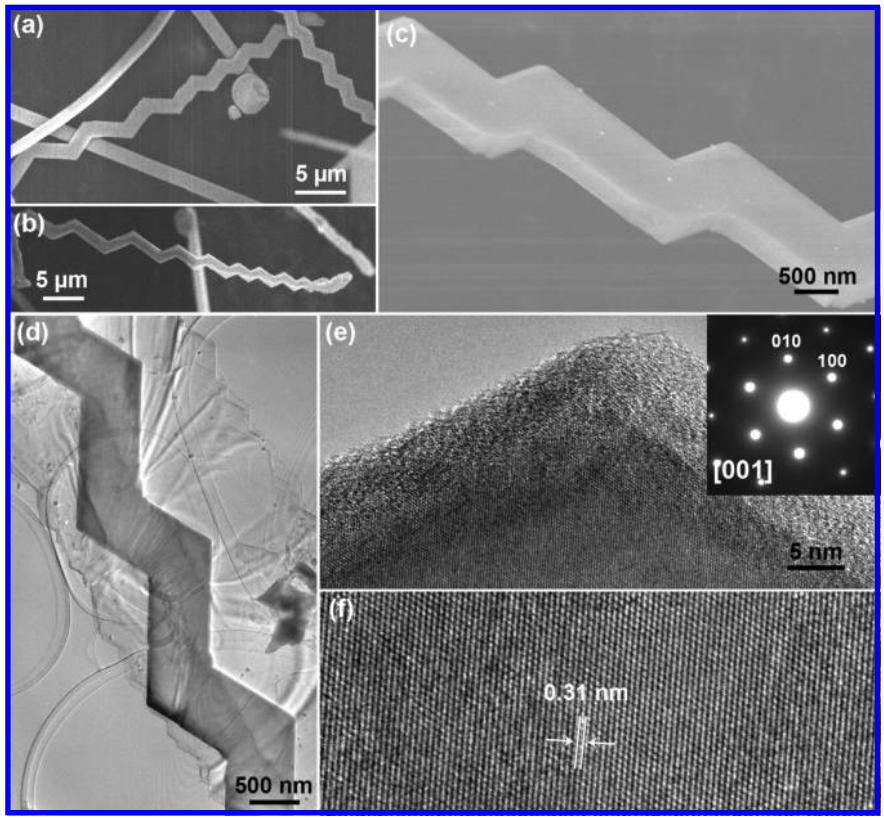

Figure 5. (a−c) SEM images, (d) TEM image, and (e,f) HRTEM images of the zigzag nanobelts. Inset in panel e is a SAED pattern.

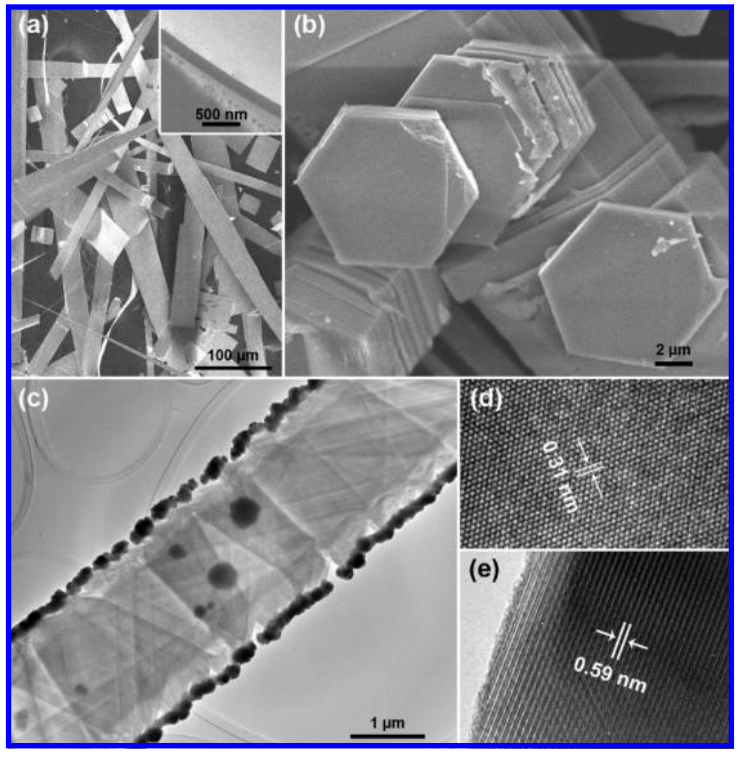

Figure 6. (a) SEM image of very long GaS microbelts; (b) SEM image of GaS hexagonal microplates; (c) TEM image of a GaS/Ga_2O_3 heterostructured nanobelt; (d,e) HRTEM images taken from the center GaS nanobelt and the outer Ga_2O_3 nanoparticles.

When the substrate temperature is 950 °C, GaS microbelts were formed instead of GaS nanobelts, as revealed by Figure 6a. The GaS product deposited at this temperature is typical GaS microbelts instead of nanobelts at lower temperature. These GaS microbelts have quite long lengths in the range of several hundred micrometers to several millimeters. Compared with the quite different lengths, the thickness of the microbelts did not change a lot between GaS microbelts and nanobelts. As indicated in the SEM image inset in Figure 6a, the thickness of a GaS microbelt is about 100 nm, only a little thicker than the GaS nanobelts (Supporting Information, Figure S3). These phenomena are usually observed for 1-D semiconductor nanostructures synthesized *via* vapor phase approaches, where high temperature favors the formation of microbelts while low temperature favors nanobelts.[24]

We found in the present vapor−solid method that 1-D GaS nanostructures or microstructures only formed when the deposition temperature is higher than 700 °C. In the case of lower substrate temperature, for example, 650 °C, only hexagonal GaS microplates were formed as shown in Figure 6b. According to this image, all the GaS microplates are of uniform hexagonal shapes with the side length of about 4 μm.

The formation of 1-D GaS nanostructures can be explained from the viewpoint of chemical reactions. When the mixture of GaN and Bi_2S_3 was used as the source, GaN thermal decomposed to generate Ga vapor at high temperature according to the following reaction.

$$2GaN \rightarrow 2Ga + N_2 \qquad (\Delta G^{\circ}_{1443K} = -309.4 \text{ kJ/mol}) \tag{1}$$

Bi_2S_3 is believed to easily decompose at high temperature to generate S vapor:

$$2Bi_2S_3 \rightarrow 4Bi + 3S_2 \qquad (\Delta G^{\circ}_{1443K} = -188.1 \text{ kJ/mol}) \tag{2}$$

The decomposition of Bi_2S_3 to generate Bi is confirmed by the fact that Bi spheres are deposited on the inner wall of quartz tube downstream (Supporting Information, Figure S4). Then, the newly generated Ga vapor and S vapor follows thermal reaction to generate GaS vapors:

$$2Ga + S_2 \rightarrow GaS \qquad (\Delta G^{\circ}_{1443K} = -70.3 \text{ kJ/mol}) \quad (3)$$

Carried by the Ar gas, GaS vapors were then transferred to the low temperature region and deposited on the graphite substrates. Influenced by the substrate temperature, 1-D GaS nanostructures with different morphologies were then formed at different regions. GaS microbelts were formed at high temperature region and only GaS nanobelts formed at lower temperature region, which is in agreement with previous reports.[24,25] When the deposition temperature is lower than 700 °C, the growth is mainly governed by the crystal structure of hexagonal GaS phase, thus only hexagonal GaS microplates are formed. In the double quartz tube reaction system, trace GaS vapors was trapped at the upstream end of the small quartz tube, resulting in the formation of thin GaS nanowires at this point. Here, we should mention that the products were only formed in the double-tube furnace system. Without the small tube, only GaS micro- or nanoparticles are formed.

We are also able to synthesize GaS/Ga_2O_3 heterostructured nanobelts using the vapor−solid method by choosing the mixture of Ga_2O_3 and Bi_2S_3 as the evaporation source (Supporting Information, Figure S5). Figure 6c depicts a TEM image of a single GaS/Ga_2O_3 heterostructured nanobelt with a width of about 2 μm. The clear ripplelike contrast in the TEM image is due to the strain resulting from the ribbon bending.[25−27] The clear brightness contrast between the nanobelt and the surface of the nanobelt, dark nanoparticles, indicates the formation of heterostructures. EDS analysis confirms that the inner nanobelt within the heterostructures is GaS, while the outer nanoparticles are Ga_2O_3 (Supporting Information, Figure S6). We took HRTEM analysis on both the inner nanobelt and the outer nanoparticles and the images are demonstrated in Figure 6d,e. The lattice fringe in Figure 6d is calculated to be 0.31 nm, perfectly matching the (101) lattice plane of hexagonal GaS, which is in agreement with the GaS nanobelts synthesized from the mixture of GaN and Bi_2S_3. The HRTEM image taken from outer sheathed Ga_2O_3 nanoparticles is depicted in Figure 6e and the resolved lattice distance is 0.59 nm, corresponding to the (002) plane of monoclinic Ga_2O_3 phase.

In the case of using the mixture of Ga_2O_3 and Bi_2S_3, Ga_2O_3 decomposes at high temperature according to the following reactions:[21]

$$Ga_2O_3 + 2C \rightarrow Ga_2O + 2CO \qquad (\Delta G^{\circ}_{1443K} = -103.4 \text{ kJ/mol}) \quad (4)$$

$$2Ga_2O + 4CO \rightarrow 4Ga + C + 3CO_2 \qquad (\Delta G^{\circ}_{1443K} = -214.2 \text{ kJ/mol}) \quad (5)$$

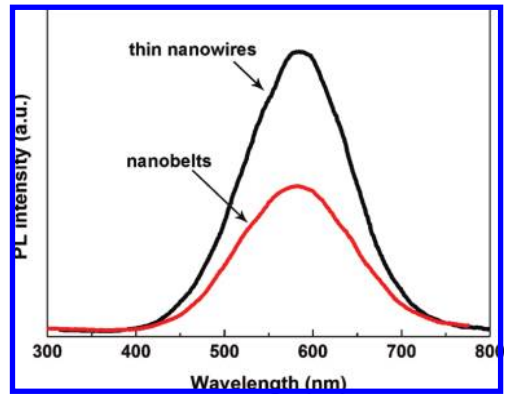

Figure 7. PL spectra of (a) thin GaS nanowires and (b) GaS nanobelts.

As revealed by the reactions 4, the total entropy considerably increases to form gaseous Ga_2O and CO. At a temperature as high as 1443 K, Ga_2O_3 spontaneously reacts with a carbon powder to form first gaseous Ga_2O and CO, and then gaseous Ga due to negative Gibbs free energy. The newly generated Ga or Ga_2O then reacts with S vapor or CS_2 to generate GaS vapors following eq 3 or the following equation:

$$Ga_2O + CS_2 \rightarrow 2GaS + CO \qquad (\Delta G^{\circ}_{1443K} = -80.4 \text{ kJ/mol}) \quad (6)$$

After the growth of GaS nanobelts, excessive Ga_2O_3 will be evaporated and deposit on the surface of GaS nanobelts, resulting in the formation of GaS/Ga_2O_3 heterostructured nanobelts.

Optical properties of the vapor−solid synthesized GaS nanostructures were also investigated. Figure 7 shows the room-temperature photoluminescence (PL) spectra taken from thin GaS nanowires and GaS nanobelts. It is clear that a strong emission centered at ~580 nm is detected in both spectra. The emission band is in agreement with the PL emission band observed from bulk GaS crystals.[28,29] This emission may come from some impurities existed in the products and is due to the radiative recombination of electrons from minimum of conduction band by holes from deep captor centers.

CONCLUSIONS

In conclusion, a simple catalyst-free vapor-solid method was developed for the controlled growth of high-quality 1-D GaS nanostructures (thin nanowires, nanobelts, zigzag nanobelts), microstructures (microbelts and hexagonal microplates), and heterostructures (GaS/Ga_2O_3 heterostructured nanobelts). We easily achieved control of products by choosing the substrate temperature and source material. These high-quality 1-D GaS nanostructures may find applications in nanoscale devices. Choosing suitable experimental parameters, such as evaporation source, deposition temperature, this simple vapor−solid method may be

extended to synthesize 1-D nanostructures of other III−VI group semiconductors.

METHODS

The vapor−solid method utilized consists of a horizontal tube furnace with two different-sized quartz tubes as shown in Scheme 1. In a typical process, the source materials, either the mixture of GaN and Bi_2S_3 (for the synthesis of 1-D GaS nano- and microstructures) or the mixture of Ga_2O_3 and Bi_2S_3 (for the synthesis of GaS/Ga_2O_3 heterostructured nanobelts) were placed in a graphite boat in the center of the furnace. High purity Ar (99.999%) gas was used as the carrier gas. After purging the furnace with Ar gas for 30 min, the temperature of the furnace was increased to 1170 °C and kept at that temperature for 1 h. Graphite plates (length × width: 2 cm × 0.5 cm) were used as the substrates for the growth of GaS products. After cooling down to room temperature, yellow powders were found deposited on the graphites substrates as well as the open entrance of the small quartz tube. Different kinds of GaS products were grown on graphite substrates placed downstream at different locations with different temperatures (Scheme 1).

The produced GaS samples were characterized using an X-ray powder diffractometer (RINT 2200), a Hitachi field-emission scanning electron microscope (SEM, S-4800), a JEOL field-emission scanning electron microscope (SEM, JSM-6700F), and a JEOL 300 KV field-emission transmission electron microscope (TEM, JEM-3000F) equipped with energy dispersive X-ray spectrometry (EDS). Photoluminescence (PL) was studied at room temperature by using a continuous-wave He−Cd laser with a 325 nm line.

Acknowledgment. The authors acknowledge financial support from the High-Level Talent Recruitment Foundation of Huazhong University of Science and Technology, the L.K. Whittier Foundation, and the National Science Foundation (CCF-0726815 and CCF-0702204).

Supporting Information Available: Low-magnification SEM image of thin GaS nanowires, EDS spectrum taken from thin GaS nanowires, high-magnification SEM image of a GaS microbelt, SEM image of Bi spheres deposited at the low temperature region, SEM image and EDS spectra of the GaS/Ga_2O_3 heterostructured nanobelts. This material is available free of charge *via* the Internet at http://pubs.acs.org.

REFERENCES AND NOTES

1. Lieth, R. M. A. *Preparation and Crystal Growth of Materials with Layered Structures*; Reidel, D., Ed.; Reidel: Dordrecht, Holland, 1977.
2. Aono, T.; Kase, K.; Kinoshita, A. Near-Blue Photoluminescence of Zn-Doped GaS Single Crystals. *J. Appl. Phys.* **1993**, *74*, 2818–2820.
3. Xin, Q. S.; Conrad, S.; Zhu, X. Y. The Deposition of a GaS Epitaxial Film on GaAs Using an Exchange Reaction. *Appl. Phys. Lett.* **1996**, *69*, 1244–1246.
4. Huang, Y.; Duan, X.; Wei, Q.; Lieber, C. M. Directed Assembly of One-Dimensional Nanostructures into Functional Networks. *Nature (London)* **2001**, *291*, 630–633.
5. Huang, M.; Mao, S.; Feick, H.; Yan, H.; Wu, Y.; Kind, H.; Weber, E.; Russo, R.; Yang, P. D. Room-Temperature Ultraviolet Nanowire Nanolasers. *Science* **2001**, *292*, 1897–1899.
6. Xia, Y.; Yang, P. D.; Sun, Y.; Wu, Y.; Mayer, B.; Gates, B.; Yin, Y.; Kim, F.; Yan, H. One-Dimensional Nanostructures: Synthesis, Characterization, and Applications. *Adv. Mater.* **2003**, *15*, 353–389.
7. Bae, S. Y.; Seo, H. W.; Park, J.; Yang, H.; Park, J. c.; Lee, S. Y. Single-Crystalline Gallium Nitride Nanobelts. *Appl. Phys. Lett.* **2002**, *81*, 126–128.
8. Tenne, R.; Margulis, L.; Genut, M.; Hodes, G. Polyhedral and Cylindrical Structures of Tungsten Disulphide. *Nature (London)* **1992**, *360*, 444–446.
9. Shen, G. Z.; Chen, P. C.; Bando, Y.; Golberg, D.; Zhou, C. Bicrystal Nanobelts of Cd3P2 and Zn3P2 and Their Electric Transport Properties. *Chem. Mater.* **2008**, *20*, 7319–7323.
10. Ng, H. T.; Li, J.; Smith, M. K.; Nguyen, P.; Cassell, A.; Han, J.; Meyyappan, M. Growth of Epitaxial Nanowires at the Junctions of Nanowalls. *Science* **2003**, *300*, 1249.
11. Shen, G. Z.; Bando, Y.; Golberg, D. Recent Developments in Single-Crystal Inorganic Nanotubes Synthesised from Removable Templates. *Int. J. Nanotechnol.* **2007**, *4*, 730–749.
12. Lu, W.; Ding, Y.; Chen, Y.; Wang, Z. L.; Fang, J. Bismuth Telluride Hexagonal Nanoplatelets and Their Two-Step Epitaxial Growth. *J. Am. Chem. Soc.* **2005**, *127*, 10112–10116.
13. Shen, G. Z.; Bando, Y.; Golberg, D. Synthesis and Structures of High-Quality Single-Crystalline II_3-V_2 Semiconductors Nanobelts. *J. Phys. Chem. C* **2007**, *111*, 5044–5049.
14. Lu, W.; Gao, P.; Jian, W. B.; Wang, Z. L.; Fang, J. Perfect Orientation Ordered *in-Situ* One-Dimensional Self-Assembly of Mn-Doped PbSe Nanocrystals. *J. Am. Chem. Soc.* **2004**, *126*, 14816–14812.
15. Shen, G. Z.; Bando, Y.; Ye, C.; Yuan, X.; Sekiguchi, T.; Golberg, D. Single-Crystalline Nanotubes of II_3-V_2 Semiconductors. *Angew. Chem., Int. Ed.* **2006**, *45*, 7568–7572.
16. Tian, B.; Zheng, X.; Kempa, T. J.; Fang, Y.; Yu, N.; Yu, G.; Huang, J.; Lieber, C. M. Coaxial Silicon Nanowires as Solar Cells and Nanoelectronic Power Sources. *Nature (London)* **2007**, *449*, 885–890.
17. Shen, G. Z.; Chen, D. Self-Coiling of $Ag_2V_4O_{11}$ Nanobelts into Perfect Nanorings and Microloops. *J. Am. Chem. Soc.* **2006**, *128*, 11762–11763.
18. Kohler, T.; Frauenheim, T.; Hajnal, Z.; Seifert, G. Tubular Structures of GaS. *Phys. Rev. B* **2004**, *69* (1−3), 193403.
19. Gautam, U. J.; Vivekchand, S. R. C.; Govindaraj, A.; Kulkarni, G. U.; Selvi, N. S.; Rao, C. N. R. Generation of Onions and Nanotubes of GaS and GaSe Through Laser and Thermally Induced Exfoliation. *J. Am. Chem. Soc.* **2005**, *127*, 3658–3659.
20. Hu, P.; Liu, Y.; Fu, L.; Cao, L.; Zhu, D. B. GaS Multi-Walled Nanotubes from the Lamellar Precursor. *Appl. Phys. A* **2005**, *80*, 1413–1417.
21. Hu, J.; Bando, Y.; Zhan, J. H.; Liu, Z. W.; Golberg, D. Uniform and High-Quality Submicrometer Tubes of GaS Layered Crystals. *Appl. Phys. Lett.* **2005**, *87* (1−3), 153112.
22. Xu, F. F.; Hu, J.; Bando, Y. Tubular Configurations and Structure-Dependent Anisotropic Strains in GaS Multi-Walled Sub-microtubes. *J. Am. Chem. Soc.* **2005**, *127*, 16860–16865.
23. Panda, S. K.; Datta, A.; Sinha, G.; Chaudhuri, S.; Chavan, P. G.; Patil, S. S.; More, M. A.; Joag, D. S. Synthesis of Well-Crystalline GaS Nanobelts and Their Unique Field Emission Behavior. *J. Phys. Chem. C* **2008**, *112*, 6240–6244.
24. Shen, G. Z.; Bando, Y.; Liu, B.; Tang, C.; Huang, Q.; Golberg, D. Systematic Investigation of the Formation of 1D α-Si_3N_4 Nanostructures by Using a Thermal-Decomposition/Nitridation Process. *Chem.—Eur. J.* **2006**, *12*, 2987–2993.
25. Dong, L. F.; Jiao, J.; Coulter, M.; Love, L. Catalytic Growth of CdS Nanobelts and Nanowires on Tungsten Substrates. *Chem. Phys. Lett.* **2003**, *376*, 653–658.
26. Pan, Z. W.; Dai, Z. R.; Wang, Z. L. Nanobelts of Semiconducting Oxides. *Science* **2001**, *291*, 1947–1949.
27. Cao, X. B.; Xie, Y.; Zhang, S. Y.; Li, F. Q. Ultra-Thin Trigonal Selenium Nanoribbons Developed From Series-Wound Beads. *Adv. Mater.* **2004**, *16*, 649–653.
28. Chiricenco, V.; Caraman, M.; Rusu, I. I.; Leontie, L. On the Luminescence of GaS(Cu) Single Crystals. *J. Lumin.* **2003**, *101*, 71–77.
29. Aydinli, A.; Gasanly, N. M.; Goksen, K. Donor−Acceptor Pair Recombination in Gallium Sulfide. *J. Appl. Phys.* **2000**, *88*, 7144–7149.